Intrapellet Diffusivities from TAP Pulse Responses via Moment-Based Analysis

A. H. J. Colaris, J. H. B. J. Hoebink, M. H. J. M. de Croon, and J. C. Schouten
Eindhoven University of Technology, Laboratory of Chemical Reactor Engineering,
5600 MB Eindhoven, The Netherlands

Moment-based analysis was applied to determine successfully inter- and intrapellet diffusion coefficients from experimental TAP outlet pulse responses over a one-zone bed with porous particles. Different temperatures, gas molar masses, and pellet sieve fractions were used to validate the Knudsen diffusion relation for inert gases inside porous catalyst pellets. The zeroth to third moments of the outlet pulse response were analytically derived for rectangular, cylindrical and spherical pellets. The third moment provides a significantly more accurate access to the intrapellet diffusivity than the second moment does. The experimental window of the TAP reactor is explored for porous silica as catalyst support bed filling. The relevance of concentration gradients inside the pellet is illustrated with model simulations.

Introduction

Steady-state kinetic experiments are usually carried out for their relative simplicity in determining reaction-rate equations and the corresponding rate coefficients involved in chemical reactions. Transient kinetics, however, play an important role in understanding the underlying reaction mechanisms. Transient experiments have the advantage of providing more information about the possible intermediates involved in a sorption or reaction mechanism, as well as about the rate coefficients of the related elementary steps. Different kinds of transients can be studied (Bennett, 2000), among them concentration pulse responses, cycling of the feed (Silveston, 1998), and isotopic switches (Happel, 1986). Temporal analysis of products (TAP) is an important method in the category of pulse-response techniques, which is performed at low pressures in a fixed-bed reactor, where Knudsen diffusion is the transport mechanism (Gleaves et al., 1988). The TAP reactor system was originally created to assist the catalyst development process. Improvements have been made from then on by adding extra mass spectrometer analysis, as is the case with the MultiTracK reactor setup (Nijhuis, 1998), and by optimizing the detection sensitivity as realized with the TAP-2 reactor setup (Gleaves et al., 1997).

TAP has been extensively applied in experimental studies on catalytic reaction mechanisms and other surface processes (Kopinke et al., 1992; Coulson et al., 1993; Buyevskaya et al., 1994; Mallens et al., 1994; Weerts et al., 1996; Schuurman et al., 1997; Heitnes Hofstad et al., 1997; Pantazidis et al., 1998; Heneghan et al., 1999; Mills et al., 1999; Dewaele et al., 1999) and the method has been numerically evaluated or simulated (Soick et al., 2000; Hinz et al., 2000).

Determination of diffusivities in zeolites was discussed by Nijhuis et al. (1999) and Keipert and Baerns (1998) in relation to TAP experiments. They used surface diffusion as the transport mechanism in the micropores to describe their experimental results.

The use of moment-based analysis (MBA) to evaluate TAP pulse experiments has been addressed for some particular cases. MBA is characterized by the total number of unknown parameters to be assessed from one pulse-response curve. For n parameters, the descriptions of the zeroth to the nth moments of the outlet pulse-response curve are needed. For a one-zone reactor filled with nonporous catalyst pellets, where the gaseous components undergo adsorption and desorption at one type of site, assuming first-order desorption kinetics, the zeroth and first moment in relation to the adsorbant and the zeroth moment in relation to the product, are known (Gleaves et al., 1988). The zeroth moment is related to the conversion, the first moment to the average residence time. The thin-zone reactor model for TAP pulse-response experiments was mathematically applied to irreversible adsorption/reaction for the zeroth and first moment, and to re-

Correspondence concerning this article should be addressed to J. H. B. J. Hoebink.

versible adsorption for the zeroth to second moment (Shekhtman et al., 1999a). The analytical solution for the first moment in relation to the mean residence time of a nonreacting gas in a three-zone TAP reactor packed with nonporous pellets was briefly presented by Phanawadee et al. (1999). Yablonsky et al. (1998) formulated the MBA theory for (pseudo-)linear TAP models corresponding to (pseudo-) first-order reactions. Here, CO oxidation over platinum powder was taken as an example. Zou et al. (1994) presented the first moment for porous pellets. They mention that the second moment does not exist, which is valid only in the case of very slow intrapellet diffusion, comparable to a situation of nonporous pellets.

Besides analytical treatment, MBA was also used in actual TAP experiments (Lafyatis et al., 1997; Creten et al., 1995). In the case of reversible adsorption on nonporous pellets, the zeroth to second moments were also derived (Huinink, 1995). Here, porous pellets were considered for cases of extremely slow and fast intrapellet diffusion.

An attempt was made by Shekhtman et al. (1999b) to unravel the zeroth to second moments for intra- and interpellet diffusion in porous media, assuming rectangular pellets. In the following sections, this porous pellet model is theoretically corrected and elaborated in great detail, as well as experimentally validated. The TAP pulse experiments and the relevant properties of the used porous pellets are described in the experimental characterization section. In the theory section, continuity equations for both inter- and intrapellet diffusion of inert gases are combined to describe the nth moments ($n = 0,1,2,3$) for beds of porous rectangular, cylindrical, and spherical pellets. Experimental data on inter- and intrapellet diffusivities are verified for the Knudsen relation with respect to temperature, molar mass, and pellet size.

Experimental Characterization

TAP pulse experiment

The experiments were carried out in an original TAP setup (Gleaves et al., 1988). Subsequent single pulses were admitted to the inlet of the TAP reactor at time intervals ranging between 1 and 3 s, depending on the necessary detection time for the complete outlet pulse signal in order to obtain all information for applying MBA. The inlet pulse size was typically $2 \cdot 10^{15}$ molecules, which guarantees Knudsen transport conditions on the interpellet level. The pulsed gas was either argon or a mixture of inert gases. Some inert gas concentrations were as low as 2 vol. %, which required to repeat the inlet pulse a hundred times in order to improve the signal-to-noise ratio in the outlet pulse response by signal averaging.

Pellet properties

Table 1 shows the physical properties of a 2 wt. % Pt/SiO_2 catalyst and the corresponding silica support (Colaris et al., 1999). The data of the latter were used in the current TAP experiments, MBA, and model simulations. Both materials were provided by Engelhard de Meern BV (The Netherlands). SEM pictures of the materials showed the pellets to be almost ideally spherical. XRD measurements indicated a polymorph structure of silica.

Table 1. Physical Properties of Porous Silica Pellets Used as Bed Material

Material	d_{pel} (μm)	ϵ_{total}	ϵ^*_{pel}	ϵ_b	d^*_{pore} (nm)	Surf. Area* BET (m^2/g)
2 wt. % Pt/SiO_2	150–212	0.85	0.76	0.38	32 ± 7	120
SiO_2	150–212	0.85	0.74	0.42	37 ± 7	114
	212–250		0.74		35 ± 7	120
	425–500		0.74		35 ± 7	108

*Obtained by N_2 physisorption.

MBA of TAP Pulse Responses from Beds of Porous Pellets

When performing TAP pulse experiments over beds of porous catalysts under ultrahigh vacuum (UHV) conditions, one needs to account for Knudsen diffusion as transport mechanism, both on the scale of the bed and on the scale of the porous pellets. The corresponding two continuity equations, describing Knudsen diffusion in the bed and in the pellet, should be coupled in order to obtain expressions for the pulse-response moments involved in MBA.

Interpellet diffusion

Interpellet Knudsen diffusion describes the pulse transport on the bed scale:

$$\epsilon_b \frac{\partial C_b(x,t)}{\partial t} = D_{e,b} \frac{\partial^2 C_b(x,t)}{\partial x^2} + (1-\epsilon_b) a_v N_{pel}. \quad (1)$$

Transforming the variables x and t into dimensionless numbers, $z = x/\ell_b$ and $\tau = t/t_b$ with $t_b = \epsilon_b \cdot \ell_b^2/D_{e,b}$, gives the equation

$$\frac{\partial C_b}{\partial \tau} = \frac{\partial^2 C_b}{\partial z^2} + (1-\epsilon_b) \frac{\ell_b^2}{D_{e,b}} a_v N_{pel}. \quad (2)$$

Intrapellet diffusion

In the case of pellets with mesopores, transport in the pellets can be described with Knudsen diffusion as well. The corresponding continuity equation depends on the geometry of the catalyst pellet. Three pellet shapes are considered in detail: rectangular, cylindrical, and spherical pellets.

Rectangular Pellets. Diffusion of inert gases inside a pellet with a rectangular shape is described by

$$\epsilon_p \frac{\partial C_p(y,t)}{\partial t} = D_{e,p} \frac{\partial^2 C_p(y,t)}{\partial y^2}. \quad (3)$$

Transformation of the variables y and t into dimensionless numbers, $\rho = r/R$, with $2R$ being the thickness of the rectangular pellet, and $\tau = t/t_b$ with $t_p = \epsilon_p \cdot R^2/D_{e,p}$, gives the following equation:

$$\frac{\partial C_p}{\partial t} = \frac{t_b}{t_p} \frac{\partial^2 C_p}{\partial \rho^2}. \quad (4)$$

Laplace transformation (Kreyszig, 1993) of this equation, using $C_p(\tau,\rho) \rightarrow \overline{C}_p\ (s,\rho)$, with $\alpha = t_b/t_p$, leads to

$$\frac{s\overline{C}_p}{\alpha} = \frac{\partial^2 \overline{C}_p}{\partial \rho^2} \tag{5}$$

The general solution of Eq. 5 is given by

$$\overline{C}_p = b_1 \cdot \sinh\left(\sqrt{\frac{s}{\alpha}} \cdot \rho\right) + b_2 \cdot \cosh\left(\sqrt{\frac{s}{\alpha}} \cdot \rho\right). \tag{6}$$

Using the following boundary conditions

$$\left.\frac{\partial \overline{C}_p}{\partial \rho}\right|_0 = 0 \tag{7}$$

and

$$\overline{C}_p\big|_1 = \overline{C}_b, \tag{8}$$

for the Laplace transform one obtains $\overline{N}|_1$ of the flux N_{pel}, through the outer pellet surface

$$\overline{N}|_1 = \frac{D_{e,p}}{R}\left.\frac{\partial \overline{C}_p}{\partial \rho}\right|_1 = \frac{D_{e,p}}{R}\overline{C}_b\sqrt{\frac{s}{\alpha}} \cdot \tanh\left(\sqrt{\frac{s}{\alpha}}\right). \tag{9}$$

Transforming the interpellet continuity equation (Eq. 2) into the Laplace domain and combining it with Eq. 9, results in

$$s\overline{C}_b - C_b(\tau = 0) = \frac{\partial^2 \overline{C}_b}{\partial z^2} - \left[\frac{(1-\epsilon_b)\,\ell_b^2 a_v}{D_{e,b}}\right]\frac{D_{e,p}}{R}\sqrt{\frac{s}{\alpha}}\tanh\left(\sqrt{\frac{s}{\alpha}}\right)\cdot\overline{C}_b. \tag{10}$$

Assuming a Dirac δ_z-pulse as the starting condition, with pulse size N_{ps} and cross-sectional area A_s of the TAP reactor bed, Eq. 10 is rewritten as

$$\frac{\partial^2 \overline{C}_b}{\partial z^2} = (f+s)\cdot\overline{C}_b - \frac{N_{PS}}{\epsilon_b A_s\,\ell_b}\delta_z, \tag{11}$$

where for a rectangular pellet, f is defined as the following function of s

$$f(s) = \left[\frac{(1-\epsilon_b)\,\ell_b^2 a_v}{D_{e,b}}\right]\frac{D_{e,p}}{R}\sqrt{\frac{s}{\alpha}}\tanh\left(\sqrt{\frac{s}{\alpha}}\right). \tag{12}$$

We now apply a second Laplace transformation to Eq. 11

$$q^2\breve{\overline{C}} - q\overline{C}_b(z=0) - \left.\frac{\partial \overline{C}_b}{\partial z}\right|_{Z=0} = (f+s)\cdot\breve{\overline{C}}_b - \frac{N_{PS}}{\epsilon_b A_s\,\ell_b}, \tag{13}$$

with

$$\overline{C}_b(z,s) = \int_0^\infty C_b e^{-st}\,d\tau \tag{14}$$

and

$$\breve{\overline{C}}_b(q,s) = \int_0^\infty \overline{C}_b e^{-qz}\,dz. \tag{15}$$

By applying the boundary conditions

$$\overline{C}_b\big|_{z=0} = \beta(s) \tag{16}$$

and

$$\left.\frac{\partial \overline{C}_b}{\partial z}\right|_{z=0} = 0, \tag{17}$$

Eq. 13 is written as

$$\left[q^2 - (f+s)\right]\cdot\breve{\overline{C}}_b = -\frac{N_{PS}}{\epsilon_b A_s\,\ell_b} + q\beta. \tag{18}$$

Introducing $T_{ps} = N_{ps}/(\epsilon_b A_s\,\ell_b)$, one obtains

$$\breve{\overline{C}}_b = \frac{\frac{1}{2}\left(\beta + \frac{T_{ps}}{\sqrt{(f+s)}}\right)}{q+\sqrt{(f+s)}} + \frac{\frac{1}{2}\left(\beta - \frac{T_{ps}}{\sqrt{(f+s)}}\right)}{q-\sqrt{(f+s)}}, \tag{19}$$

which is turned into $\overline{C}_b$ by inverse Laplace transformation

$$\overline{C}_b = \frac{1}{2}\left(\beta + \frac{T_{ps}}{\sqrt{(f+s)}}\right)e^{-\sqrt{(f+s)}\cdot z} + \frac{1}{2}\left(\beta - \frac{T_{ps}}{\sqrt{(f+s)}}\right)e^{+\sqrt{(f+s)}\cdot z} = \beta\cdot\cosh\left(\sqrt{(f+s)}\cdot z\right) - \frac{T_{ps}}{\sqrt{(f+s)}}\cdot\sinh\left(\sqrt{(f+s)}\cdot z\right). \tag{20}$$

With

$$\overline{C}_b\big|_{z=1} = 0 \tag{21}$$

as the boundary condition at the end of the bed, β can be written as a function of s

$$\beta(s) = \frac{T_{ps}}{\sqrt{(f+s)}}\cdot\tanh\sqrt{(f+s)}\,. \tag{22}$$

To determine the Laplace-transformed molar flow at the outlet of the TAP reactor, $\overline{F}|_1$, the general equation for the Laplace transform of the concentration in the bed (Eq. 20), in combination with the explicit representation of $\beta(s)$ shown in Eq. 22, gives

$$\overline{F}|_1 = -\frac{A_s D_{e,b}}{\ell_b}\left.\frac{\partial \overline{C}_b}{\partial z}\right|_1 = \frac{A_s D_{e,b}}{\ell_b}\frac{T_{ps}}{\cosh\sqrt{(f+s)}}. \tag{23}$$

The specific influence of the pellet geometry is represented by $f(s)$ (Eq. 12), which contains $a_v = 1/R$ for the case of rectangular pellets.

Cylindrical pellets. The continuity equation for cylindrical pellets is

$$\epsilon_p \frac{\partial C_p(r,t)}{\partial t} = D_{e,p} \frac{1}{r} \frac{\partial}{\partial r}\left[r \frac{\partial C_p(r,t)}{\partial r} \right]. \tag{24}$$

Again, transforming the variables r and t into dimensionless numbers, $\rho = r/R$ and $\tau = t/t_b$ with $t_p = \epsilon_p \cdot R^2/D_{e,p}$ gives the following equation

$$\frac{\partial C_p}{\partial \tau} = \frac{t_b}{t_p} \frac{1}{\rho} \frac{\partial}{\partial \rho}\left[\rho \frac{\partial C_p}{\partial \rho} \right]. \tag{25}$$

Using Laplace transformation $C_p(\tau,\rho) \rightarrow \overline{C}_p(s,\rho)$, we get, with $\alpha = t_b/t_p$

$$\frac{s\overline{C}_p}{\alpha} = \frac{1}{\rho} \frac{\partial}{\partial \rho}\left[\rho \frac{\partial \overline{C}_p}{\partial \rho} \right] \tag{26}$$

or

$$\rho^2 \frac{\partial^2 \overline{C}_p}{\partial \rho^2} + \rho \frac{\partial \overline{C}_p}{\partial \rho} - \frac{s}{\alpha} \rho^2 \overline{C}_p = 0. \tag{27}$$

The general solution to Eq. 27 is given by modified Bessel functions of the first (I_n) and second (K_n) kind (Abramowitz and Stegun, 1970; Spiegel, 1974), with order $n = 0$

$$\overline{C}_p = c_1 I_o\left(\sqrt{\frac{s}{\alpha}} \cdot \rho \right) + c_2 K_o\left(\sqrt{\frac{s}{\alpha}} \cdot \rho \right), \tag{28}$$

with

$$I_n(x) = i^{-n} J_n(ix) = e^{-n\pi i/2} J_n(ix) \tag{29}$$

and

$$K_n(x) = \begin{cases} \dfrac{\pi}{2} \dfrac{I_{-n}(x) - I_n(x)}{\sin(n\pi)} & n \neq 0,1,2,3,\ldots \\ \lim\limits_{v \to n} \dfrac{\pi}{2} \dfrac{I_{-p}(x) - I_p(x)}{\sin(v\pi)} & n = 0,1,2,3,\ldots, \end{cases} \tag{30}$$

where

$$J_n(x) = x^n \sum_{m=0}^{\infty} \frac{(-1)^m x^{2n}}{2^{2m+n} m!(n+m)!}. \tag{31}$$

The boundary conditions are

$$\overline{C}_p\big|_0 : \text{finite value} \Rightarrow c_2 = 0 \tag{32}$$

and

$$\overline{C}_p\big|_1 = \overline{C}_b \Rightarrow c_1 = \frac{\overline{C}_b}{J_0\left(\sqrt{\frac{s}{\alpha}} \right)}. \tag{33}$$

The Laplace transform $\overline{N}|_1$ for pellet flux N_{pel} is obtained from Eqs. 28–33:

$$\overline{N}|_1 = \frac{D_{e,p}}{R} \frac{\partial \overline{C}_p}{\partial \rho}\bigg|_1 = \frac{D_{e,p}}{R} \overline{C}_b \sqrt{\frac{s}{\alpha}} \cdot \frac{J_1\left(\sqrt{\frac{s}{\alpha}} \right)}{J_0\left(\sqrt{\frac{s}{\alpha}} \right)}. \tag{34}$$

Combining the Laplace transform of Eq. 2 with Eq. 34, results in

$$s\overline{C}_b - C_b(\tau = 0) = \frac{\partial^2 C_b}{\partial z^2} - \left[\frac{(1-\epsilon_b)\, \ell_b^2 a_v}{D_{e,b}} \right] \frac{D_{e,p}}{R} \sqrt{\frac{s}{\alpha}} \cdot \frac{J_1\left(\sqrt{\frac{s}{\alpha}} \right)}{J_0\left(\sqrt{\frac{s}{\alpha}} \right)} \cdot \overline{C}_b, \tag{35}$$

which is the equivalent of Eq. 10. Similar manipulation as for rectangular coordinates again leads to Eq. 11. Function f, however, is now defined as

$$f(s) = \left[\frac{(1-\epsilon_b)\, \ell_b^2 a_v}{D_{e,b}} \right] \frac{D_{e,p}}{R} \sqrt{\frac{s}{\alpha}} \cdot \frac{J_1\left(\sqrt{\frac{s}{\alpha}} \right)}{J_0\left(\sqrt{\frac{s}{\alpha}} \right)}. \tag{36}$$

The rest of the procedure to obtain an expression for the flux at the outlet of the TAP reactor is also similar to the case of the rectangular pellet. The same equation (Eq. 23) is obtained. For the case of cylindrical pellets, the influence of the pellet geometry is herein represented by $f(s)$ from Eq. 36, with $a_v = 2/R$.

Spherical pellets. For spherical pellets, the equivalent of the Laplace transformed continuity equation (Eq. 27) is

$$\rho^2 \frac{\partial^2 \overline{C}_p}{\partial \rho^2} + 2\rho \frac{\partial \overline{C}_p}{\partial \rho} - \frac{s}{\alpha} \rho^2 \overline{C}_p = 0. \tag{37}$$

Substituting $\overline{C}_p = g(\rho)/\rho$ in Eq. 38 gives the general solution for $g(\rho)$, and subsequently

$$\overline{C}_p = d_1 \frac{\sinh\left(\sqrt{\frac{s}{\alpha}} \cdot \rho \right)}{\rho} + d_2 \frac{\cosh\left(\sqrt{\frac{s}{\alpha}} \cdot \rho \right)}{\rho}. \tag{38}$$

Here we use identical boundary conditions as in cylindrical pellets:

$$\overline{C}_p\big|_0 : \text{finite value} \Rightarrow d_2 = 0 \tag{39}$$

and

$$\overline{C}_p\big|_1 = \overline{C}_b \Rightarrow d_1 = \frac{\overline{C}_b}{\sinh\left(\sqrt{\frac{s}{\alpha}} \right)}. \tag{40}$$

The Laplace transform $\overline{N}|_1$ of the flux at the outer pellet surface is now

$$\overline{N}|_1 = \frac{D_{e,p}}{R}\left.\frac{\partial \overline{C}_p}{\partial \rho}\right|_1 = \frac{D_{e,p}}{R}\overline{C}_b\left(\frac{\sqrt{\frac{s}{\alpha}}}{\tanh\sqrt{\frac{s}{\alpha}}} - 1\right). \quad (41)$$

Similar reasoning again leads to Eq. 11, with f now defined as

$$f(s) = \left[\frac{(1-\epsilon_b)\,\ell_b^2 a_v}{D_{e,b}}\right]\frac{D_{e,p}}{R}\left(\frac{\sqrt{\frac{s}{\alpha}}}{\tanh\sqrt{\frac{s}{\alpha}}} - 1\right), \quad (42)$$

which represents the type of pellets with $a_v = 3/R$ in the case of spherical pellets.

MBA as an analytical tool

Determination of the moments of the pulse response function is straightforward from here on

$$M_n = \int_0^\infty F\cdot t^n\,dt = t_b^{n+1}\int_0^\infty F\cdot \tau^n\,d\tau = (-1)^n \lim_{s\to 0}\frac{\partial^n \overline{F}|_1}{\partial s^n}. \quad (43)$$

When differentiating Eq. 43 n times to obtain expressions for the zeroth to nth moments, the molar flow $\overline{F}|_1$ (Eq. 23) can be approximated by a Taylor polynome of at least $(n+1)$th order in s, without loss of accuracy. For a reactor bed filled with rectangular, cylindrical, or spherical pellets, the expressions for the first to the third moments are shown in Table 2. In these relations, τ_b and τ_p are represented by

$$\tau_b = \frac{\epsilon_b\cdot \ell_b^2}{D_{e,b}}\cdot(1+\Delta) \quad (45)$$

$$\tau_p = \frac{\epsilon_p\cdot R^2}{D_{e,p}}\cdot\frac{\Delta}{(1+\Delta)}, \quad (46)$$

with

$$\Delta = \epsilon_p\cdot\frac{(1-\epsilon_b)}{\epsilon_b}. \quad (47)$$

The zeroth moment is defined as the pulse size, N_{ps}. The first moment provides information about the interpellet diffusion time, τ_b, and the effective interpellet diffusion coefficient, $D_{e,b}$, while additional information about the intrapellet diffusion time, τ_p, and the effective intrapellet diffusion coefficient, $D_{e,p}$, is obtained from the second moment. The third moment seems redundant, as it contains the same information as the second moment. The relative weight of the intrapellet diffusion in the third moment, however, is considerably larger than in the second moment. This allows a more accurate assessment of the intrapellet diffusivity, in particular, if τ_p is small.

Numerical simulation of pulse responses

TAP pulse simulations were performed for a bed of porous pellets in order to compare experimental and predicted pulse responses. DSS002 subroutines (Sibeli and Schiesser, 1992) were used to obtain discretization with respect to the axial bed coordinate and the radial pellet coordinate. The reactor bed consists of one zone, which was divided into 41 equidistant gridpoints. On the pellet scale, 11 equidistant gridpoints were applied. The resulting ordinary differential equations (ODE) were integrated in time by using the D02NCF routine from the NAG Fortran Library Manual (NAG Ltd., 1997).

Results

The integrands $F\cdot t^n$ of the zeroth up to the third moment are shown in Figure 1. The situation of $n = 0$ is equal to the measured outlet pulse-response signal. Smoothing or other pulse manipulation was not applied except adaptation of the base line. This base-line adaptation is necessary because of an offset signal, caused by the electronic equipment of the TAP setup, which becomes significant at very low signal values, in particular when evaluating the higher moments. The adaptation of the base line is chosen such that the contribution to all moments ($n = 0,1,2,3$) of the last 10% of the time interval relevant for the signal is less than 2%

$$\frac{M_n[\text{last 10\% in time}]}{M_n[\text{total}]} = \frac{\int_{0.9\Delta t}^{\Delta t} F\cdot t^n\,dt}{\int_0^{\Delta t} F\cdot t^n\,dt} \le 2\%, \quad (48)$$

with Δt the total time of signal monitoring.

For the situation shown in Figure 1, this means that $\Delta t =$ 1.4 s. The integrands of the second and third moment do not approach a limit value of zero at high t values. This is caused by scatter in the data, which becomes enhanced at high t by multiplication of the signal with t^2 or t^3. The nonrandom-like

Table 2. First vs. Third Moments*

Particle Shape	M_1/M_0	M_2/M_0	M_3/M_0
Rectangular	$\tau_b/2$	$(1/2)\cdot\tau_b[(5/6)\cdot\tau_b + (2/3)\cdot\tau_p]$	$(1/2)\cdot\tau_b\cdot[(61/60)\cdot\tau_b^2 + (5/3)\cdot\tau_b\cdot\tau_p + (4/5)\cdot\tau_p^2\cdot(1+\Delta)/(\Delta)]$
Cylindrical	$\tau_b/2$	$(1/2)\cdot\tau_b[(5/6)\cdot\tau_b + (1/4)\cdot\tau_p]$	$(1/2)\cdot\tau_b\cdot[(61/60)\cdot\tau_b^2 + (5/8)\cdot\tau_b\cdot\tau_p + (1/8)\cdot\tau_p^2\cdot(1+\Delta)/(\Delta)]$
Spherical	$\tau_b/2$	$(1/2)\cdot\tau_b[(5/6)\cdot\tau_b + (2/15)\cdot\tau_p]$	$(1/2)\cdot\tau_b\cdot[(61/60)\cdot\tau_b^2 + (1/3)\cdot\tau_b\cdot\tau_p + (4/105)\cdot\tau_p^2\cdot(1+\Delta)/(\Delta)]$

*See Eqs. 45, 46, and 47 for τ_b, τ_p, and Δ, respectively.

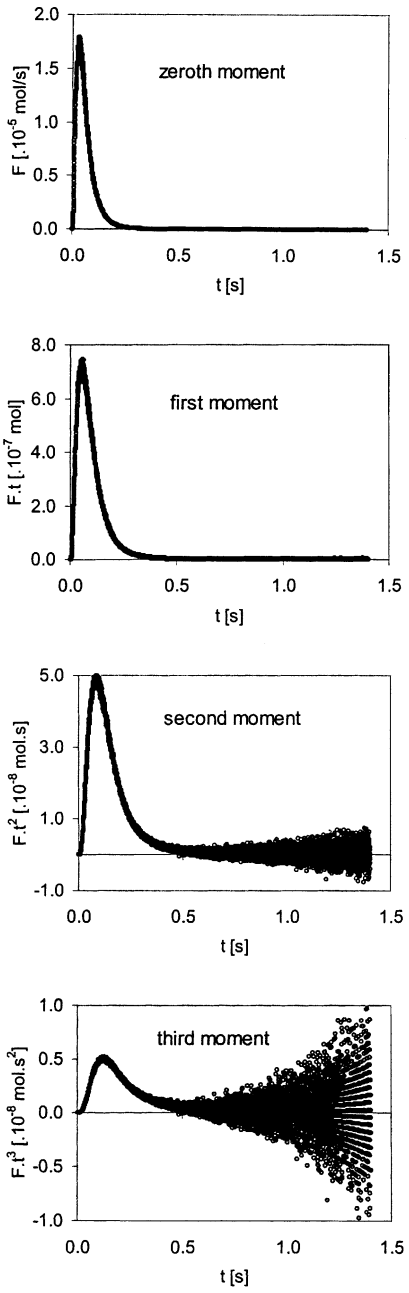

Figure 1. Integrands $F \cdot t^n$ for $n = 0,1,2,3$, as calculated from the experimental outlet pulse response of Ar pulsed over porous silica.

Bed length $l_b = 19$ mm; sieve fraction $d_{SiO_2} = 425-500$ μm; $T = 373$ K.

behavior of the third moment at the end of the experiment is caused by digitalization of the outlet pulse signal by the TAP data-acquisition equipment.

From the integrands shown in Figure 1, one can conclude —for this specific situation—that a relatively large amount of information is included at the end of the pulse. Although measuring the pulse over $\Delta t = 0.3$ s would seem sufficient, one has to conclude from the third moment that a signal over at least $\Delta t = 0.6$ s has to be considered in order to prevent loss of information about intrapellet diffusion.

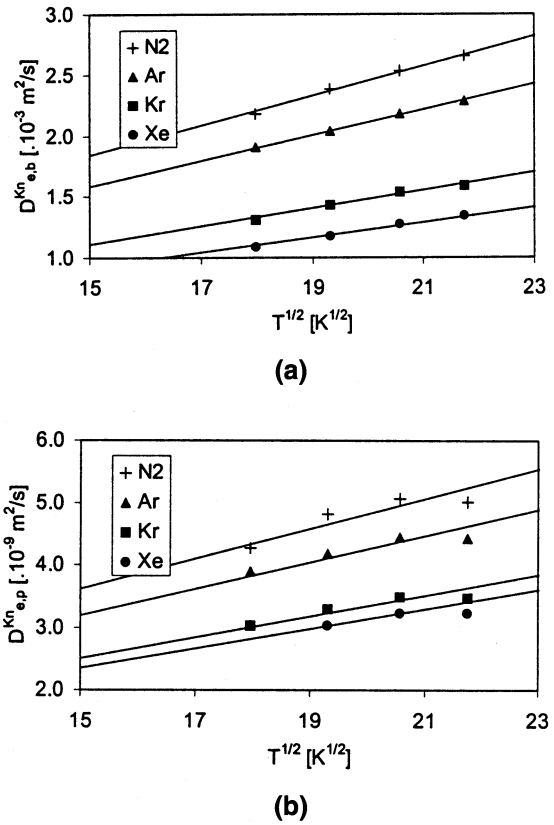

Figure 2. Interpellet diffusivity (a) and intrapellet diffusivity (b) as a function of $T^{1/2}$.

Results are obtained via MBA of outlet pulse responses of 82.8 vol. % N_2, 11.8 vol. % Ar, 1.8 vol. % Kr, and 1.8 vol. % Xe pulsed as a mixture over porous silica pellets (bed length $l_b = 38$ mm, sieve fraction $d_{SiO_2} = 212-250$ μm, $T = 323$, 373, 423, and 473 K). The lines in both (a) and (b) parts are linear fits through the origin.

Effective inter- and intrapellet diffusivities for several inert gases, obtained from the first and third moments, respectively, are shown in Figure 2 as a function of $T^{1/2}$. The lines in the figure are linear fits through the origin for the individual inert gases, indicating a $T^{1/2}$ temperature relationship for diffusion in both bed and pellet. The same inter- and intrapellet diffusivities are shown in Figure 3, but now as a function of $M^{-1/2}$. The lines represent linear fits for the individual temperatures, indicating that the diffusivity in both bed and pellet is well proportional to $M^{-1/2}$. For the intrapellet diffusivities (Figure 3b), the linear fits do not go through the origin.

A second set of experiments was carried out by pulsing Ar over a porous silica bed with bed length $l_b = 19$ mm and pellet sieve fraction $d_{SiO_2} = 425-500$ μm at $T = 373$, 573, 773 and 973 K. At the two lower temperatures, the results were in line with the Knudsen relation. At the two higher temperatures, the results were not as expected. At $T = 773$ K, the intrapellet diffusion was about two times smaller than the expected value. When Eq. 48 was applied to the optimization of the baseline, the contribution of the last part of the response would not fall below a value of 10% for the third moment. At $T = 973$ K, the diffusivity could not be estimated at all from the third moment, since the peak area between 0

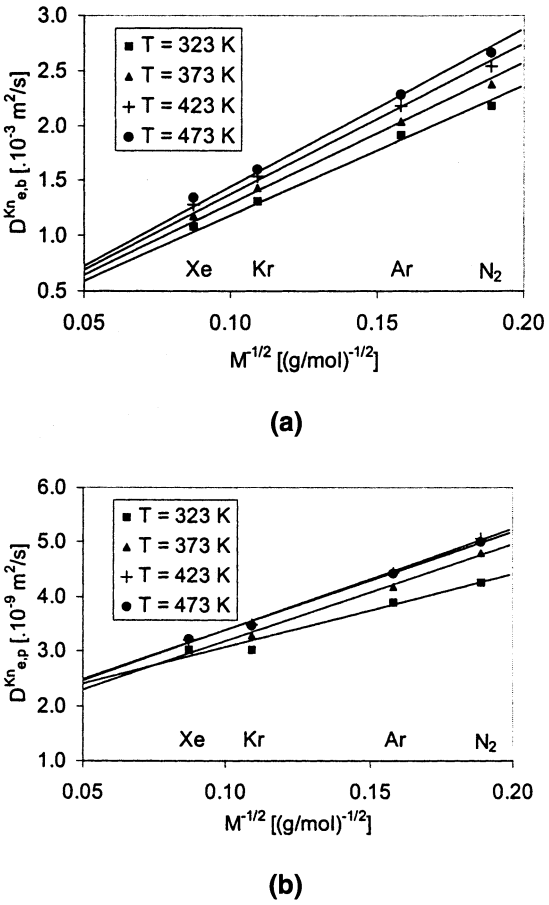

Figure 3. Interpellet diffusivity (a) and intrapellet diffusivity (b) as a function of $M^{-1/2}$.

Experimental conditions are the same as mentioned in Figure 2. The lines in part (a) are linear fits going through the origin. The lines in part (b) are linear fits that do not go through the origin.

and 0.5 s was almost zero. It could be possible that the signals were not recorded for a sufficiently long time, as diffusion into larger pellets takes more time. It cannot be excluded that temperature gradients affect the high-temperature results, as it is complicated to maintain a uniform temperature in the TAP reactor at high temperatures (Huinink, 1995; Weerts, 1995). The fact that diffusivities obey the Knudsen relation at lower temperatures (see Figures 2 and 3) indicates that temperature gradients have a negligible influence at those temperatures. Different bed lengths do not influence the value of the diffusivity, but a shorter bed length improves the signal-to-noise ratio of the response.

Discussion

The intrapellet diffusivities calculated from the second moment showed a less reliable result than when the third moment was used. This is because the contribution of the intrapellet diffusion compared to interpellet diffusion in the ratio M_3/M_0 is relatively high and in the ratio M_2/M_0 low. For example, the intrapellet contribution in the ratio M_3/M_0 for spherical pellets is given by $(1/3)\cdot\tau_b\cdot\tau_p+(4/105)\cdot\tau_p^2\cdot(1+\Delta)/(\Delta)$ and the interpellet contribution by $(61/60)\cdot\tau_b^2$, as can be seen in Table 2. The first term in the intrapellet contribution is predominant; thus, (1/3):(61/60), which is over 1:3, is the ratio of intra- to interpellet contributions for the third moment. The intrapellet contribution in the ratio M_2/M_0 is represented by $(2/15)\tau_p$, while the interpellet contribution is $(5/6)\tau_b$, which causes the ratio of intra- to interpellet contribution (2/15):(5/6) to be about 1:6 for the second moment.

Although the interpellet diffusivity as determined from the first moment is relatively well conditioned, the error in its value is carried over in the second and also the third moment, which causes an inaccuracy in the estimation of the intrapellet diffusivity. This would argue that a different experimental approach be used, one that assesses the interpellet diffusivity separately from the pulse experiments over similar, but nonporous, pellets, and the subsequent use of its value for the determination of the intrapellet diffusivity over porous pellets. In this way errors in the interpellet diffusivity, which may arise from intrapellet diffusion, are avoided. It is emphasized here that attempts to simultaneously assess both diffusivities from nonlinear regression of the full TAP pulse response were unsuccessful. A similar approach to obtain the intrapellet diffusivity via regression of the full response, after the interpellet diffusivity was determined independently via pulse experiments over nonporous pellets, gave rather inaccurate results.

Effective diffusivities are related to the Knudsen diffusivity via

$$D_e^{Kn}=\frac{\epsilon}{\tilde{\tau}}D^{Kn}, \tag{49}$$

while for the latter the following relation holds

$$D^{Kn}=\frac{d_i}{3}\sqrt{\frac{8R_{\text{gas}}T}{\pi M}}\,. \tag{50}$$

The results of Figures 2 and 3 show that not only the interpellet diffusivity obeys the Knudsen relation concerning the dependence on temperature and molecular weight, as is already known (Gleaves et al., 1988), but that the relation in this respect can also be applied for the intrapellet diffusivity. The linear fits of the molar mass at different temperatures in Figure 3b do not go through the origin, which indicates that there is an additional mechanism of intrapellet gas transport present. It goes beyond the scope of this article to discuss the kind of mechanism involved.

The dependence of the interpellet diffusivity on the mean pellet size is found to be also in line with the Knudsen relation for the two sieve fractions applied here. For the intrapellet diffusivity one would expect that both sieve fractions would show the same value, in particular because it was verified, from nitrogen physisorption experiments, that both fractions have nearly the same pore-size distribution, pellet porosity, and BET surface area (Table 1). The experimentally obtained values for the intrapellet diffusivities were 4.2×10^{-9} m^2/s and 1.3×10^{-8} m^2/s for the smaller and the larger sieve fractions, respectively, which could indicate a difference in tortuosity between small and large pellets (see Eq. 49). Tortuosity factors have been reported to vary between 2 and 10 (Satterfield, 1970).

When the Knudsen relation is applied in the current situation to extrapolate experimentally obtained interpellet diffusivities toward intrapellet diffusivities, one should account for the difference in pellet and pore diameters, and the difference in bed and pellet porosities. Typically, estimated values of the intrapellet diffusivities are a factor of 10 to 50 larger than the experimental intrapellet diffusivities. This would imply that the tortuosity of the intrapellet pores is much larger than the tortuosity of the interstitial bed voidage. Thus, estimating the intrapellet diffusion coefficient (2×10^{-7} m^2/s) from the Knudsen relation, using the interpellet diffusion coefficient (1×10^{-3} m^2/s) and the characteristic interstitial void dimensions ($d_{\text{pore}} = 4\times10^{-8}$ m, respectively, $d_{\text{pel}} = 2\times10^{-4}$ m) is not accurate enough. Pore distributions and a different tortuosity on the intrapellet scale seem to influence in a non-negligible manner (Satterfield, 1970).

The relevance of concentration gradients inside the pellets is illustrated in Figure 4. Here, the behavior of the intrapellet concentration is simulated as a function of time for pellets near the inlet and the outlet of the reactor bed ($z = 1/40$ and $z = 39/40$, and $\rho = 0$, 0.1, 0.5, 0.9, and 1). It is seen in Figure 4 that pulses traveling through the bed lead, over a short period of time, to high concentrations in the outer regions of a pellet, while low concentrations in the inner pellet parts last much longer. Pellets near the bed entrance show profiles at much higher concentration levels than pellets near the bed outlet, in line with the broadening of the pulse admitted to the bed. It is clear that admission of a pulse causes severe intrapellet concentration gradients. One might expect that such a situation would be enhanced if additional processes like adsorption and desorption and/or catalytic reactions would occur. The fact that the number of molecules in a typical TAP pulse is of an order of magnitude of 1% of the number of active sites in the reactor, should be considered in this context. Depletion of the pulse may result in only parts of the bed, or even only parts of some pellets, being actually involved in catalytic processes.

The conditions of TAP experiments can be varied by changing the size of the catalyst pellets, the length of the bed filling, and the operating temperature. Thus, the experimental window for assessment of intrapellet diffusivities is determined both by the physical transport properties of the reactor bed and catalyst pellet, and by the detection sensitivity of the TAP equipment under given experimental conditions. One might estimate the influence of the physical transport properties by using the third moment from Table 2. For this purpose, the integrand is to be split into an interpellet-induced contribution (A_b) and an intrapellet-induced contribution (A_p)

$$A_b = (61/60)\cdot\tau_b^2 \tag{51}$$

and

$$A_p = (1/3)\cdot\tau_b\cdot\tau_p + (4/105)\cdot\tau_p^2\cdot(1+\Delta)/(\Delta). \tag{52}$$

To estimate the boundaries of the experimental window, one might assume that at least 5% of each contribution should be present in the third moment

$$5\% \le (A_p)/(A_p + A_b) \le 95\% \tag{53}$$

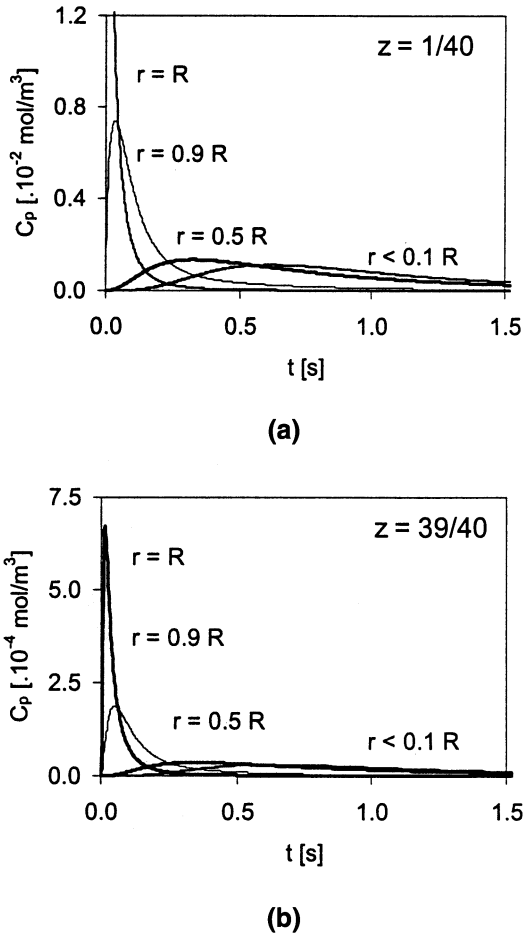

Figure 4. Simulated intrapellet concentrations (C_p) of Ar at $T = 373$ K as a function of time at $z = 1/40$ (a) and $z = 39/40$ (b) in the TAP reactor bed with the dimensionless spherical pellet coordinate as parameter: $\rho = 1$, 0.9, 0.5, 0.1, and 0.

The silica bed length is 19 mm and the pellet sieve fraction is 425–500 μm. Note the different vertical scales. Values of the inter- and intrapellet diffusivity are 2×10^{-3} and 2×10^{-9} m^2/s, respectively.

Using the expressions mentioned in Eqs. 45–47 in combination with the bed and pellet properties in Table 1, the following estimation can be derived

$$1.52 \le \frac{D_{e,b}}{D_{e,p}}\cdot\frac{d_{\text{pel}}^2}{\ell_b^2} \le 128 \tag{54}$$

The bed length is restricted by the size of the TAP reactor, which is about 40 mm maximum, and by ideal plug-flow conditions ($l_b/d_{\text{pel}} > 50$) (Froment and Bischoff, 1990), which is about 5 mm minimum. The size of the catalyst pellet is also restricted, on the one hand by ideal plug-flow conditions ($d_{\text{reactor}}/d_{\text{pel}} > 10$) (Froment and Bischoff, 1990), corresponding to a pellet size of about 560 μm as the maximum diameter, and on the other hand, by a mesh size of the removable stainless-steel screen at the end of the reactor. In our case, 100 μm is the minimum pellet diameter.

Beside the bed properties, detection limits are also relevant. Choosing a larger pellet diameter ($d_{SiO_2} = 425-500\ \mu m$) and a smaller bed length ($l_b = 19$ mm) showed an experimental detection limit at $T \geq 773$ K. Here, the information of the second and third moments is much less than the white noise causing oscillations at the end of the time interval of the moment concerned. The applied base line adaptation (Eq. 48) was not sufficient for obtaining reliable intrapellet diffusivities at these extreme experimental conditions. There should have been an additional demand that the integrands of the second and third moments have the same order of magnitude as the white noise in the last 10% of the measured time interval.

Simulation of the TAP experiments with diffusivities obtained from MBA indicates intrapellet concentration gradients. These same gradients were already assumed to be present in the silica support material at an earlier stage (Colaris et al., 1999).

Conclusions

Interpellet and intrapellet diffusivities were experimentally assessed with the TAP reactor via pulse experiments. The Knudsen relation was confirmed for mesoporous pellets. The data were derived from the pulse responses via moment based analysis. It is concluded that use of the third moment is more reliable for obtaining intrapellet diffusivities, when compared to the use of the second moment. Model simulations with the experimentally obtained diffusivities reveal large concentration gradients within the pellets.

Acknowledgments

The Dutch Foundation for Scientific Research, Chemical Sciences Section (NWO-CW) is gratefully acknowledged for their financial support.

Notation

A_b = interpellet contribution of the integrand of the third moment, dimensionless
A_p = intrapellet contribution of the integrand of the third moment, dimensionless
A_s = cross-sectional area of the TAP reactor bed, m^2
a_V = pellet surface area per pellet volume, m^{-1}
b_1, b_2 = constants used in the general solution of the Laplace transformed diffusion equation in regard to rectangular pellets, Eq. 6, mol/m^3
c_1, c_2 = constants used in the general solution of the Laplace transformed diffusion equation in regard to cylindrical pellets, Eqs. 32 and 33, mol/m^3
C = concentration, mol/m^3
$\bar{C}$ = Laplace transformed concentration $t \rightarrow s$, mol/m^3
$\bar{\bar{C}}$ = Laplace transformed concentration $t \rightarrow s$ and $z \rightarrow q$, mol/m^3
d = diameter, m
d_1, d_2 = constants used in the general solution of the Laplace transformed diffusion equation in regard to spherical pellets, Eqs. 39 and 40, mol/m^3
d_i = interstitial voids diameter, m
D = diffusion coefficient, m^2/s
f = pellet-type dependent function, dimensionless
F = molar flow, mol/s
i = complex number, dimensionless
I_n = modified Bessel function of the first kind of order n, dimensionless
J_n = Bessel function of the first kind of order n, dimensionless
K_n = modified Bessel function of the second kind of order n, dimensionless
ℓ = length, m
m = nonnegative integer, dimensionless
M = molar mass, kg/mol
M_n = nth moment, mol·s^n
n = nonnegative integer, dimensionless
N = molar flux, mol/m^2·s
N_{pel} = molar flux at outer pellet boundary, mol/m^2·s
N_{ps} = pulse size, mol
q = Laplace transformation of coordinate z, dimensionless
r = place coordinate of the cylindrical/spherical pellet, m
R = half-thickness of a pellet, m
R_{gas} = gas constant, J/mol·K
s = Laplace transformed of time t, s^{-1}
t = time, s
Δt = total time of TAP pulse outlet signal monitoring, s
t_b = characteristic interpellet diffusion time, s
t_p = characteristic intrapellet diffusion time, s
T = temperature, K
T_{ps} = pulse concentration, mol/m^3
x = place coordinate of the reactor bed, m
y = place coordinate of the rectangular pellet, m
z = place coordinate of the reactor bed, dimensionless

Greek letters

α = ratio of the characteristic interpellet (bed) diffusion time and the characteristic intrapellet (pellet) diffusion time, dimensionless
β = Laplace transformed boundary condition at the beginning of the TAP reactor bed filled with rectangular pellets, mol/m^3
δ_z = Dirac delta function of coordinate z, dimensionless
Δ = ratio of pellet void (intrapellet volume) fraction to bed void (interpellet volume) fraction, dimensionless
ϵ = porosity, dimensionless
ν = nonnegative integer, dimensionless
ρ = pellet coordinate, dimensionless
τ = characteristic interpellet diffusion time, dimensionless
$\tilde{\tau}$ = tortuosity, dimensionless
τ_b = moment-related interpellet diffusion time, s
τ_p = moment-related intrapellet diffusion time, s

Superscripts and subscripts

Kn = Knudsen
b = bed, interpellet
e = effective
p,pel = pellet, intrapellet

Abbreviations

MBA = moment based analysis
TAP = temporal analysis of products
UHV = ultrahigh vacuum

Literature Cited

Abramowitz, M., and I. A. Stegun, *Handbook of Mathematical Functions*, Dover, New York (1970).

Bennett, C. O., "Experiments and Processes in the Transient Regime for Heterogeneous Catalysis," *Adv. Catal.*, **44**, 329 (2000).

Buyevskaya, O. V., M. Rothaemel, H. W. Zanthoff, and M. Baerns, "Transient Studies on the Role of Oxygen Activation in the Oxidative Coupling of Methane over Sm_2O_3, Sm_2O_3/MgO, and MgO Catalytic Surfaces," *J. Catal.*, **150**, 71 (1994).

Colaris, A. H. J., J. H. B. J. Hoebink, and J. C. Schouten, "CO Oxidation Over a Supported Pt Catalyst: Transient Kinetics Using Temporal Analysis of Products (TAP)," *Stud. Surf. Sci. Catal.*, **122**, 93 (1999).

Coulson, D. R., P. L. Mills, K. Kourtakis, P. W. J. G. Wijnen, J. J. Lerou, and L. E. Manzer, "Kinetics of the Redox Reactions of the O-2, Propylene, Gamma-Bismuth Molybdate System—a Tap Reactor Study," *Stud. Surf. Sci. Catal.*, **75**, 2015 (1993).

Creten, G., D. S. Lafyatis, and G. F. Froment, "Transient Kinetics from the Tap Reactor System—Application to the Oxidation of Propylene to Acrolein," *J. Catal.*, **154**, 151 (1995).

Dewaele, O., V. L. Geers, G. F. Froment, and G. B. Marin, "The Conversion of Methanol to Olefins—A Transient Kinetic Study," *Chem. Eng. Sci.*, **54**, 4385 (1999).

Froment, G. F., and K. B. Bischoff, *Chemical Reactor Analysis and Design*, Wiley, New York (1990).

Gleaves, J. T., J. R. Ebner, and T. C. Kuechler, "Temporal Analysis of Products (TAP)—A Unique Catalyst Evaluation System with Submillisecond Time Resolution," *Catal. Rev.-Sci. Eng.*, **30**, 49 (1988).

Gleaves, J. T., G. S. Yablonsky, P. Phanawadee, and Y. Schuurman, "TAP- 2: An Interrogative Kinetics Approach," *Appl. Catal. A*, **160**, 55 (1997).

Happel, J., *Isotopic Assessment of Heterogeneous Catalysis*, Academic Press, Orlando, FL (1986).

Heitnes Hofstad, K., J. H. B. J. Hoebink, A. Holmen, and G. B. Marin, "Partial Oxidation of Methane to Synthesis Gas over Rhodium Catalysts," *Catal. Today*, **40**, 157 (1998).

Heneghan, C. S., G. J. Hutchings, S. R. O'Laery, S. H. Taylor, V. J. Boyd, and I. D. Hudson, "A Temporal Analysis of Products Study of the Mechanism of VOC Catalytic Oxidation using Uranium Oxide Catalysts," *Catal. Today*, **54**, 3 (1999).

Hinz, A., B. Nilsson, and A. Andersson, "Simulation of Transient in Heterogeneous Catalysis: A Comparison of the Step- and Pulse-Transient Techniques for the Study of Hydrocarbon Oxidation on Metal Oxide Catalysts," *Chem. Eng. Sci.*, **55**, 4385 (2000).

Huinink, J. P., *A Quantitative Analysis of Transient Kinetic Experiments: The Oxidation of CO by O_2/NO on Pt*, PhD Thesis, Eindhoven Univ. of Technology, Eindhoven, The Netherlands (1995).

Keipert, O. P., and M. Baerns, "Determination of the Intracrystalline Diffusion Coefficients of Alkanes in H-ZSM-5 Zeolite by a Transient Technique Using the Temporal-Analysis-of-Products (TAP) Reactor," *Chem. Eng. Sci.*, **53**, 3623 (1998).

Kopinke, F. D., G. Creten, and G. F. Froment, "TAP Investigations of Selective O-Xylene Oxidation," *Stud. Surf. Sci. Catal.*, **72**, 317 (1992).

Kreyszig, E., *Advanced Engineering Mathematics*, Wiley, New York (1993).

Lafyatis, D. S., G. Creten, O. Dewaele, and G. F. Froment, "A Simple Method of Estimating Surface-Reaction Rates by Moment Analysis of TAP Reactor Pulse Experiments—Application to Benzene Hydrogenation," *Can. J. Chem. Eng.*, **75**, 1100 (1997).

Mallens, E. P. J., J. H. B. J. Hoebink, and G. B. Marin, "The Oxidative Coupling of Methane over Tin Promoted Lithium Magnesium-Oxide—A Tap Investigation," *Stud. Surf. Sci. Catal.*, **81**, 205 (1994).

Mills. P. L., H. T. Randall, and J. S. McCracken, "Redox Kinetics of $VOPO_4$ with Butane and Oxygen using the TAP Reactor System," *Chem. Eng. Sci.*, **54**, 3709 (1999).

NAG Ltd., *NAG Fortran Library Manual, Mark 18*, The Numerical Algorithms Group, Oxford (1997).

Nijhuis, T. A., *Towards a New Propene Epoxidation Process: Transient Adsorption and Kinetics Measurements Applied in Catalysis*, PhD Thesis, Delft Univ. of Technology, Delft, The Netherlands (1998).

Nijhuis, T. A., L. J. P. van den Broeke, M. J. G. Linders, J. M. van de Graaf, F. Kapteijn, M. Makkee, and J. A. Moulijn, "Measurement and Modeling of the Transient Adsorption, Desorption and Diffusion Processes in Microporous Materials," *Chem. Eng. Sci.*, **54**, 4423 (1999).

Pantazidis, A., S. A. Bucholz, H. W. Zanthoff, Y. Schuurman, and C. Mirodatos, "A TAP Reactor Investigation of the Oxidative Dehydrogenation of Propane over a V-Mg-O Catalyst," *Catal. Today*, **40**, 207 (1998).

Phanawadee, P., G. S. Yablonsky, P. Preechasanongkit, and K. Somapa, "A New Correlation for Determination of the Effective Knudsen Diffusivity of a Gas in a TAP Reactor," *Ind. Eng. Chem. Res.*, **38**, 2877 (1999).

Satterfield, C. N., *Mass Transfer in Heterogeneous Catalysis*, MIT Press, Cambridge, MA (1970).

Schuurman, Y., V. Ducarme, T. Chen, W. Li, C. Mirodatos, and G. A. Martin, "Low Temperature Oxidative Dehydrogenation of Ethane Over Catalysts Based on Group VIII Metals," *Appl. Catal. A*, **163**, 227 (1997).

Shekhtman, S. O., G. S. Yablonsky, S. Chen, and J. T. Gleaves, "Thin-Zone TAP-Reactor—Theory and Application," *Chem. Eng. Sci.*, **54**, 4371 (1999a).

Shekhtman, S. O., G. S. Yablonsky, and J. T. Gleaves, *A New Method for Determining Gas Diffusivities in the Complex Porous Media Using TAP Pulse Response Experiment*, Proc. 16th North American Catalysis Society, Boston (1999b).

Sibeli, C. A., and W. E. Schiesser, *Dynamic Modeling of Transport Process Systems*, Academic Press, San Diego, CA (1992).

Silveston, P. L., *Composition Modulation of Catalytic Reactors*, Gordon & Breach, Toronto, Ont., Canada (1998).

Soick, M., D. Wolf, and M. Baerns, "Determination of Kinetic Parameters for Complex Heterogeneous Catalytic Reactions by Numerical Evaluation of TAP Experiments," *Chem. Eng. Sci.*, **55**, 2875 (2000).

Spiegel, M. R., *Fourier Analysis*, McGraw-Hill, New York (1974).

Weerts, W. L. M., "Low Pressure CVD of Polycrystalline Silicon: Reaction Kinetics and Reactor Modelling," PhD Thesis, Eindhoven Univ. of Technology, Eindhoven, The Netherlands (1995).

Weerts, W. L. M., M. H. J. M. de Croon, and G. B. Marin, "The Adsorption of Silane, Disilane and Trisilane on Polycrystalline Silicon: A Transient Kinetic Study," *Surf. Sci.*, **367**, 321 (1996).

Yablonsky, G. S., S. O. Shekhtman, S. Chen, and J. T. Gleaves, "Moment-Based Analysis of Transient Response Catalytic Studies (TAP Experiment)," *Ind. Eng. Chem. Res.*, **37**, 2193 (1998).

Zou, B. S., M. P. Dudukovic, and P. L. Mills, "Modelling of Pulsed Gas Transport Effects in the TAP Reactor System," *J. Catal.*, **148**, 683 (1994).

Manuscript received May 17, 2001, and revision received Mar. 25, 2002.